# Classification of Fluorescent Microsphere Images Using Color

M. Soriano, L. Garcia and C. Saloma
National Institute of Physics
University of the Philippines, 1101 Diliman
Quezon City, PHILIPPINES

## Abstract

*Recent techniques in fluorescence microscopy can render objects in different colors, thus, multi-stained fluorescing samples are potential subjects for color pattern recognition. However, fluorescing microscopic samples exhibit artifacts such as photobleaching, defocus, self-illumination and scaling. This paper shows that Color Indexing, although successful with real world images, are not suitable for microscopic images. Instead, a reduced histogram binned on few major colors and a neural network for classification shows better recognition performance. Classification tests were carried out on scaled, defocused, photobleached, and combined images of AMCA (7-Amino-4-Methylcoumarin-3-Acetic Acid) and FITC (Fluorescein Isothiocynate)-stained microspheres. For Color Indexing, histograms were modeled in normalized color coordinates. Major color representatives were obtained by taking the cluster means and by Kohonen self-organizing feature map (SOM). Classification with SOM and a neural network obtained the highest overall recognition rate at 90%.*

## 1 Introduction

Recent advances in fluorescent probe manufacturing and staining techniques have permitted the multiple application of fluorophores on the same sample site resulting in the generation of a multicolored image[2],[7],[12],[9], [6],[1],[8],[14]. This capability has led to a new karyotyping method that permits for an easier and more accurate detection of chromosomal and genomic defects [9],[6],[1],[12]. Multicolor fluorescent staining has also been utilized to generate high-contrast confocal fluorescent images of internal organs in the whole-mount mouse embryo [8].

Fluorescence microscopy exhibits better sensitivity, selectivity, and precision than absorption/transmission microscopy particularly with weakly-absorbing samples which are very common in biological research. As the fluorescence marking technology further improves and finds new applications in biology and medicine (e.g. cell counting, mutation monitoring in organogenesis, imaging through a scattering medium), the availability of a rapid and accurate method to recognize and classify multicolored fluorescent images also becomes necessary.

Image classification based on color histograms distributions was first demonstrated by Swain and Ballard[13]. Their technique is inherently invariant to affine transformations in the image (rescaling, translation, rotation and perspective projection) and is also robust against the effects of partial occlusion. Schemes that improved on the histogram intersection approach of Swain, were later proposed that incorporate color constancy[4]. At low-intensity levels however, the technique is quite sensitive to noise

To our knowledge, these color object classification techniques have been demonstrated only to images of non-microscopic samples. While there exists several techniques for color pattern recognition, the images often analyzed are of large objects illuminated by natural or artificial light. Some applications include data mining in web-based applications such as in QBIC (Query By Image Content)[3] and video cut determination[15].

The classification of microscopic objects requires special attention because their images are affected by diffraction effects (defocusing, aberrations, scaling, etc) and optical noise (edge ringings, scattering, digitization errors, etc). Fluorescent objects also photobleach, that is, their efficiency to emit (fluorescent) light decreases with time for the same excitation power. The colored (fluorescent) object under consideration is also the light source itself thus the usual problem of recognition under varying background illumination conditions is absent.

In this paper, we compare the performance of color indexing, which is a classifier that uses the full histogram of the image color as the feature, versus a neural network which takes as input feature vectors based on the histogram binned to the "major colors of the fluorescent image. We show by experiments that the latter is more successful in classifying images of fluo-

rescing microspheres under varying image conditions with no fixed image size. By reducing the dimension of the color distribution and by using a neural network for classification, we may be able to reduce the effect of imaging noise and intrinsic artifacts on the classification of fluorescent images. On microscopic images degraded with random noise of different probability distributions and variances, neural networks are known to be robust classifiers[11].

In Section 2 the setup and method is discussed, while the experimental results are shown in Section 3. Section 4 summarizes our findings.

# 2 Methods

## 2.1 Images

Two fluorescent microsphere suspensions (Duke Scientific Corp) of FITC (diameter = 20 $\mu$m, excitation wavelength $\lambda_E = 490$ nm, fluorescence wavelength $\lambda_F = 520$ to 530nm) and AMCA (diameter = 10 $\mu$m, $\lambda_E = 364$ nm,$\lambda_F = 420$ nm), were viewed on separate slides using an epi-fluorescence microscope (Olympus BH2). The following objectives (Type: Dplan Apo UV) were employed: 10X (numerical aperture (NA) = 0.4,) and 40X (NA = 1.0), which are suitable for fluorescence imaging with ultraviolet light excitation. The images were captured by a CCD camera (Sony XC-711) and digitized by an 8-bit frame storeboard (DIPIX Power Grabber). Note that the camera used is only 1 CCD and therefore presents a worst case scenario in terms of imaging weak samples such as fluorospheres. The digitized images used in the experiments, were of arbitrary sizes. The four types of fluorescent objects were obtained in the following manner. The AMCA fluorospheres were observed using a dichroic mirror with a short wavelength cut-off of $\lambda_c = 420$ nm, to generate the AMCA-blue images. The FITC fluorospheres were viewed using a dichroic mirror with $\lambda_c$ = 515 nm, to produce the FITC-green images. The same FITC microspheres were also viewed with another dichroic mirror where $\lambda_c = 590$ nm, to generate the FITC-red images. Images of blank sample (no fluorosphere found in the field of view) were also obtained for the background images.

Eight classes were considered for recognition : R (red), G (green), B (blue), Bk (background), Gb (green-blue), Rg (red-green), Rb (red-blue), Rgb (red-green-blue). Combinations of spheres in the last four classes were created to simulate multifluorescing samples.

In addition, the R,G and B samples were imaged under two magnifications, 10x and 40x (SCALED), under photobleached conditions (DIMMED) and under defocused microscope setting (DEFOCUSED). The classifiers were tested on these images to determine their success rates with real fluorescent images inclusive of intrinsic and optical artifacts.

## 2.2 Color histogram in normalized space

To remove the dependence on brightness variation, the R,G and B components of the color image were transformed into normalized color coordinates: $I = (R + G + B)$, $r = R/I$ and $g = G/I$. Note that $b = B/I$ is redundant because $r + g + b = 1$. It is sufficient to describe the chromaticities of the image by two coordinates, say, r and g. A model for each of the eight classes was generated from the average histogram of 30 images from each class.

To classify by Color Indexing, the Histogram Intersection between the test and the model is calculated and the test sample is assigned to the model which gives the highest intersection. Histogram intersection is defined by:

$$D = \frac{\sum_{b=1}^{B} min(S_b, M_b)}{\sum_{b=1}^{B} M_b} \quad (1)$$

where $S$ is the sample histogram, $M$ is the model histogram, $b$ is the bin index and $B$ is the total number of bins. The r-g model histograms were discretized into $64 \times 64$ bins.

## 2.3 Reduced histogram generation

The major colors were determined by: 1)taking the Cluster Mean (CM) in r-g space, and 2) computing the Kohonen self-organizing map in truecolor space (SOM) [5]. The four unique clusters in the image set are R, G, B and Bk. The mean of each cluster is taken as one major color, thus there are four unique major colors. In SOM, a single layer network with 200 initial outputs gives the dot products of the input and the weights. Initially set to small random numbers, the weights are updated based on the internal monitoring of performance between neurons. The declared winner is the neuron that best matches the input. Similarity matching is found using the minimum Euclidean distance criterion:

$$i(\mathbf{x}) = arg_j min \|\mathbf{x(n)} - \mathbf{w_j}\| \quad (2)$$

where $i(x)$ is the index of the winning neuron, n is the iteration time, index $j = 1, 2, ...N$ is number of neurons in the lattice, and $\|.\|$ refers to the Euclidean norm of the argument vector. The winning neuron is allowed an output while the rest are not. During weight update, only the winner neuron and its neighbors are allowed to adapt. If the neurons are members of the neighborhood $L$, its weight adapts according to:

$$\mathbf{w_{new}} = \eta(\mathbf{x} - \mathbf{w_{old}}) \quad (3)$$

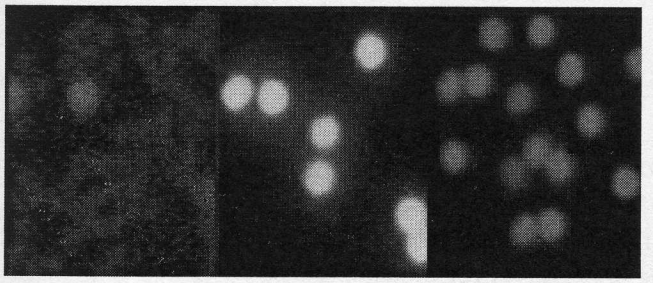

Figure 1: From left to right, AMCA, FITC-red and FITC-green.

where $\eta$ is the learning rate, otherwise, the weights remain the same. Both $\eta$ and L are functions of time. In our experiments, $\eta$ was initialized at 0.9 and then made to decrease after the first 1000 iterations until it reaches the value of 0.01. Learning is achieved when $\|\mathbf{x(n)} - \mathbf{w_j}\|$ becomes less than 0.05-a choice that is based on the assumption that there should not be too many major colors learned to avoid feature overlaps but also not too few so as to neglect the differences among colors of the same hue but of different saturation. In this manner, six major colors were obtained.

Reduced histograms were obtained as follows: The dot product of each pixel RGB with the major colors is computed and the major color with the largest product is given a one and the rest is given zero. The votes for each major color is tallied resulting in a major color histogram.

### 2.4 Neural network training

Two feedforward backpropagation networks with momentum terms were trained on 4 and 3 major colors respectively. Activation functions used were sigmoids. Desired outputs were 8-vectors corresponding to the 8 classes. Only one unit, corresponding to the class of the input, is trained to fire while the rest are trained to go to zero.

## 3 Experimental Results

Figure 1 shows an example of the fluorospheres used in this experiment. Figure 2 shows the r-g models of the eight classes considered. The cluster mean corresponds to the average r-g coordinates of the first four classes.

Tables 1 to 3 shows the confusion matrices and overall recognition rates for Color Indexing, Cluster mean + Neural network and SOM + neural network respectively. The table shows that the best performing classifier is the SOM + NN.

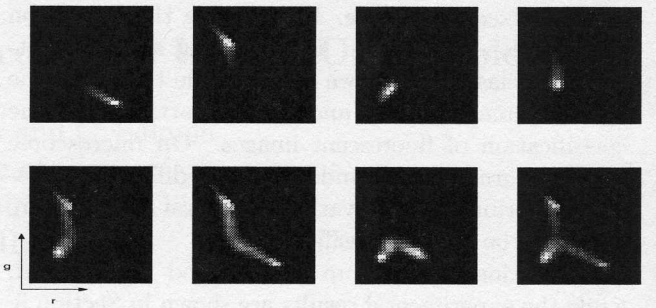

Figure 2: Histogram models in r-g space of the eight fluorescent image classes. Left to right, top to bottom R (red). G (green), B (blue), Bk (background), Gb (green-blue), Rg (red-green), (Rb (red-blue), RGB (red-green-blue).

Table 1: Confusion matrix and recognition rates (%RR) for Color Indexing.

| . | R | G | B | Bk | Gb | Rg | Rb | Rgb | %RR |
|---|---|---|---|---|---|---|---|---|---|
| R | 58 | 12 | 0 | 1 | 0 | 0 | 36 | 0 | 54 |
| G | 3 | 87 | 0 | 0 | 0 | 3 | 0 | 0 | 94 |
| B | 0 | 0 | 143 | 0 | 1 | 0 | 8 | 0 | 94 |
| Bk | 0 | 2 | 6 | 88 | 0 | 8 | 3 | 0 | 82 |
| Gb | 0 | 0 | 0 | 0 | 17 | 0 | 0 | 13 | 57 |
| Rg | 0 | 0 | 0 | 0 | 0 | 30 | 0 | 0 | 100 |
| Rb | 0 | 0 | 0 | 0 | 0 | 0 | 12 | 18 | 40 |
| Rgb | 0 | 0 | 0 | 0 | 0 | 0 | 0 | 30 | 100 |
| Total | | | | | | | | | 78 |

Table 2: Confusion matrix and recognition rates (%RR) for Cluster Mean + NN

| . | R | G | B | Bk | Gb | Rg | Rb | Rgb | % RR |
|---|---|---|---|---|---|---|---|---|---|
| R | 95 | 12 | 0 | 0 | 0 | 0 | 0 | 0 | 89 |
| G | 3 | 90 | 0 | 0 | 0 | 0 | 0 | 0 | 97 |
| B | 0 | 0 | 41 | 0 | 0 | 110 | 0 | 1 | 27 |
| Bk | 50 | 15 | 16 | 24 | 0 | 2 | 0 | 0 | 22 |
| Gb | 0 | 0 | 0 | 0 | 30 | 0 | 0 | 0 | 100 |
| Rg | 1 | 0 | 0 | 0 | 0 | 29 | 0 | 0 | 97 |
| Rb | 0 | 0 | 0 | 0 | 0 | 0 | 0 | 30 | 0 |
| Rgb | 0 | 0 | 0 | 0 | 0 | 2 | 0 | 28 | 93 |
| Total | | | | | | | | | 66 |

Table 3: Confusion matrix and recognition rates (%RR) for SOM + NN

| . | R | G | B | Bk | Gb | Rg | Rb | Rgb | % RR |
|---|---|---|---|---|---|---|---|---|---|
| R | 87 | 12 | 0 | 1 | 0 | 7 | 0 | 0 | 81 |
| G | 3 | 89 | 0 | 0 | 1 | 0 | 0 | 0 | 96 |
| B | 0 | 0 | 152 | 0 | 0 | 0 | 0 | 0 | 100 |
| Bk | 1 | 15 | 38 | 53 | 0 | 0 | 0 | 0 | 50 |
| Gb | 0 | 0 | 0 | 0 | 30 | 0 | 0 | 0 | 100 |
| Rg | 0 | 0 | 0 | 0 | 0 | 30 | 0 | 0 | 100 |
| Rb | 0 | 0 | 0 | 0 | 0 | 0 | 30 | 0 | 100 |
| Rgb | 0 | 0 | 0 | 0 | 2 | 0 | 0 | 28 | 93 |
| Total | | | | | | | | | 90 |

Table 4: Summary of recognition rates for Color Indexing (CI), Cluster Mean and Neural Networks (CM+NN) and Kohonen Self-Organizing Map plus Neural Network (SOM+NN).

| IMAGE TYPE | CI (%RR) | CM+NN (%RR) | SOM+NN (%RR) |
|---|---|---|---|
| DEFOCUSED | 47 | 92 | 95 |
| DIMMED | 86 | 88 | 98 |
| SCALED | 45 | 66 | 77 |

Next, the recognition rate is tallied for cases of photobleached, defocused and scaled images. It must be emphasized that both feature extractors and classifiers were trained using only normal images, that is, no defocused, photobleached or magnified images were included in the training set. Table 4 shows the average results for 8 classes.

Note that the best performing classifier is SOM+NN followed by CM+NN. Color Indexing shows very poor recognition except with photobleached images. The normalized r-g space used for color indexing is already independent of intensity variations thus it follows that classification of images with varied brightness will be successful in such a space.

## 4 Conclusions and Discussions

Our results show that for fluorescing samples, the best classifier is one which uses a SOM for major color extraction and a neural network for classification. Despite having been trained only on normal images, it generalized even with photobleached, magnified and defocused images. One would have expected that cluster mean and a neural network would have worked as well, however, our results prove otherwise.

Apparently, the feature space spanned by the four-component feature vector in CM is not sufficient to separate the classes. This means, there are overlaps in the clusters of classes in CM space. Table 2 shows, for example, a large confusion in class B with Rg, and Rb with Rgb. The additional major colors learned by SOM allowed a better separation as shown by the consistenly high recognition rates of SOM+NN.

Color Indexing unsatisfactorily classified defocused and scaled images even though with non-microscopic samples in [13] it performs well with low resolution images. In microscopy, the image of a point is an Airy pattern, a bright circle surrounded by concentric circles of decreasing brightness. The resolution of two adjacent points depend on the numerical aperture of the objective lens and the wavelength of light from each point. If these two points are very close, their Airy patterns overlap. Overlap becomes more severe when the microscope is defocused. Additional colors are created if the two points are of different colors. A Color Indexing classifier, if trained only on normal images, will not be able to model additional colors which may appear in defocused or scaled images.

Therefore, taking into account artifacts in microscopic imaging, unsupervised feature extraction and neural network classification are suitable tools for the classification of fluorescing microspheres.

## References


[1] S Abrams, "Fluorescent Markers: GFP Joins the Common Dyes", *Biophotonics International* Vol. 5, 48 - 54, March-April 1998.

[2] S. Andersson-Engels, J. Johansson, and S. Svanderg, "Multicolor fluorescence imaging systems for tissue diagnostics", *Proc. SPIE Bioimaging Two-Dimensional Spectroscopy* Vol. 1205, 179-189, 1990.

[3] C Faloutsos, W Equitz, M Flickner et al., "Efficient and Effective Querying by Image Content", *J. Intelligent Information Systems* Vol. 3, 231-262, 1994.

[4] B. Funt, G. Finlayson, "Color constant color indexing", *IEEE Trans.Pattern Analysis and Machine Intelligence*, Vol. 17, 522-529,1995.

[5] T. Kohonen, "The self-organizing map", *Proc IEEE*, Vol. 78, 1464-1480, 1990.

[6] L Kostrikis, S Tyagi, M Mhlanga, D Ho, R Kramer, "Spectral Genotyping of Human Alleles", *Science* Vol 279, 5354-5356, 1998.

[7] . Z Malik, S Cabib, R Buckwald , Y Garini, and D Soenksen, "A novel spectral imaging system combining spectroscopy with imaging applications for

biology", *Proc. SPIE-Opt. Imaging Tech. Biomed* Vol. 2319, 180-184, 1994.

[8] C. Saloma, C Palmes-Saloma, H Kondoh, "Site-specific confocal fluorescence imaging of biological microstructures in a turbid medium", *Phys Med Bio* Vol. 43, 1741-1759, 1998.

[9] E. Schrock, S. du Manoir, T. Veldman, B. Schoell, J. Weinberg, M.A. Ferguson-Smith, Y. Ning, D.H. Ledbetter, I. Bar-Am, D. Soenksen, Y. Garini, T. Reid, "Multicolor Spectral Karyotyping of Human Chromosomes", *Science* Vol. 273, 494-498, 1996.

[10] M Soriano and C Saloma, "Cell classification by a learning principal components analyzer and a backpropagation neural network", *Bioimaging* Vol. 3, 168-175, 1995.

[11] M. Soriano and C. Saloma, "Improved classification robustness for noisy cell images represented as principal component projections in a hybrid recognition system", *Applied Optics* Vol. 37 No. 17, 3628-3638, 1998.

[12] M. Speicher, S Gwyn Ballard, and D Ward, "Karyotyping human chromosomes by combinatorial multi-fluor FISH", *Nat Genet* Vol. 12, 368-375, 1996.

[13] M Swain, D Ballard, "Color Indexing", *Intl. J. Computer Vision* Vol. 7, 11-32, 1991.

[14] R Tsien, A Miyawaki, "Biochemical Imaging :Seeing the Machinery of Live Cells", *Science* Vol. 280, 1954-1955, 1998.

[15] B-L Yeo and B Liu, "Rapid Scene Analysis on Compressed Video", *IEEE Transactions on Circuits and Systems for Video Technology*, Vol. 5, 533-544, 1995.